

Quinoxalinophenanthrophenazine Based Cruciforms

Lucas Ueberricke,^[a, b] Dennis Mizioch,^[a] Farhad Ghalami,^[c] Felix Mildner,^[a] Frank Rominger,^[a] Thomas Oeser,^[a] Marcus Elstner,^[c] and Michael Mastalerz*^[a, b]

A series of cruciform aryl-substituted quinoxalinophenanthrophenazine derivatives (QPPs) was synthesized through Suzuki-Miyaura cross-coupling of a 2,7-diborylated pyrene tetraketal building block. The QPPs were analyzed for their optoelectronic properties by absorption and emission spectroscopy, cyclic

voltammetry and quantum-chemical calculations. The solid-state packing was investigated as well and evaluated for its charge transport properties by calculated charge transfer integrals.

Introduction

Due to their optoelectronic properties and extended π conjugated nature, quinoxalinophenanthrophenazines (QPPs) are a promising class of compounds for applications such as use as semiconductors in organic electronics, e.g., in organic field-effect transistors (OFETs),^[1–4] in organic light-emitting diodes (OLEDs)^[5–10] or in photovoltaic cells (OPVs).^[11–12] In QPPs the cross-conjugation across the pyrene rings can best be described with additional Clar sextets,^[13–14] by which an exceptionally high stability can be explained. In recent years, a great variety of QPP derivatives has been synthesized in order to modify optoelectronic properties, solid state packing and solubility.^[15–46] To adjust optoelectronic properties of QPPs, various electron-donating or -withdrawing substituents were introduced to the QPP backbone, but to the best of our knowledge exclusively on the peripheral rings fused with the pyrazine units, rather than at remaining positions of the pyrene core.^[18–19,22,28–29,47–49] Although e.g. HOMO- and LUMO levels can be adjusted by these derivations, in almost all cases either both HOMO and LUMO levels are destabilized or stabilized for each QPP, because orbital nodes are found for both frontier molecular orbitals on

the same atoms of the QPP backbone typically along the longitudinal axis.^[22,41–42,49]

Cruciforms are X-shaped conjugated compounds where HOMOs and LUMOs are located on different arms of the molecule and orbital nodes of both are overlapping only at the crossing of these two arms.^[50–54] Therefore, by placing substituents on the different arms, HOMO or LUMO levels can be adjusted more or less independently, allowing a broader variety in FMO level and optical gap adjustment.^[52]

We envisioned to synthesize QPP-based cruciforms and to the best of our knowledge the only QPP with substituents at the pyrene core are based on the 2,7-diiodo pyrene tetraketal **1**, that has previously been introduced by Mateo-Alonso and coworkers as a versatile building block for the synthesis of TIPS-ethynyl substituted QPPs and other pyrene fused azaacenes (Scheme 1).^[17,19,22] However the TIPS-ethynyl substituents acted more as solubilizing units, rather than contributing to the electronic levels of the frontier molecular orbitals. Electron

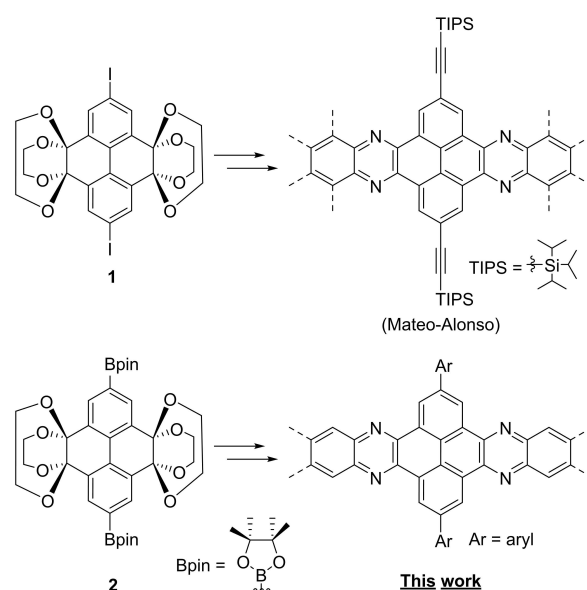
[a] Dr. L. Ueberricke, D. Mizioch, F. Mildner, Dr. F. Rominger, Dr. T. Oeser, Prof. Dr. M. Mastalerz
Organisch-Chemisches Institut
Ruprecht-Karls-Universität Heidelberg
Im Neuenheimer Feld 270, 69120 Heidelberg, Germany
E-mail: michael.mastalerz@oci.uni-heidelberg.de

[b] Dr. L. Ueberricke, Prof. Dr. M. Mastalerz
Centre for Advanced Materials (CAM)
Ruprecht-Karls-Universität Heidelberg
Im Neuenheimer Feld 225, 69120 Heidelberg, Germany

[c] F. Ghalami, Prof. Dr. M. Elstner
Institut für Physikalische Chemie
Karlsruher Institute of Technology (KIT)
Kaiserstr. 12, 76131 Karlsruhe, Germany

Supporting information for this article is available on the WWW under <https://doi.org/10.1002/ejoc.202100701>

© 2021 The Authors. European Journal of Organic Chemistry published by Wiley-VCH GmbH. This is an open access article under the terms of the Creative Commons Attribution Non-Commercial NoDerivs License, which permits use and distribution in any medium, provided the original work is properly cited, the use is non-commercial and no modifications or adaptations are made.



Scheme 1. Synthesis of TIPS-ethynyl substituted QPPs (Mateo-Alonso)^[17,19,22] and aryl substituted QPPs.

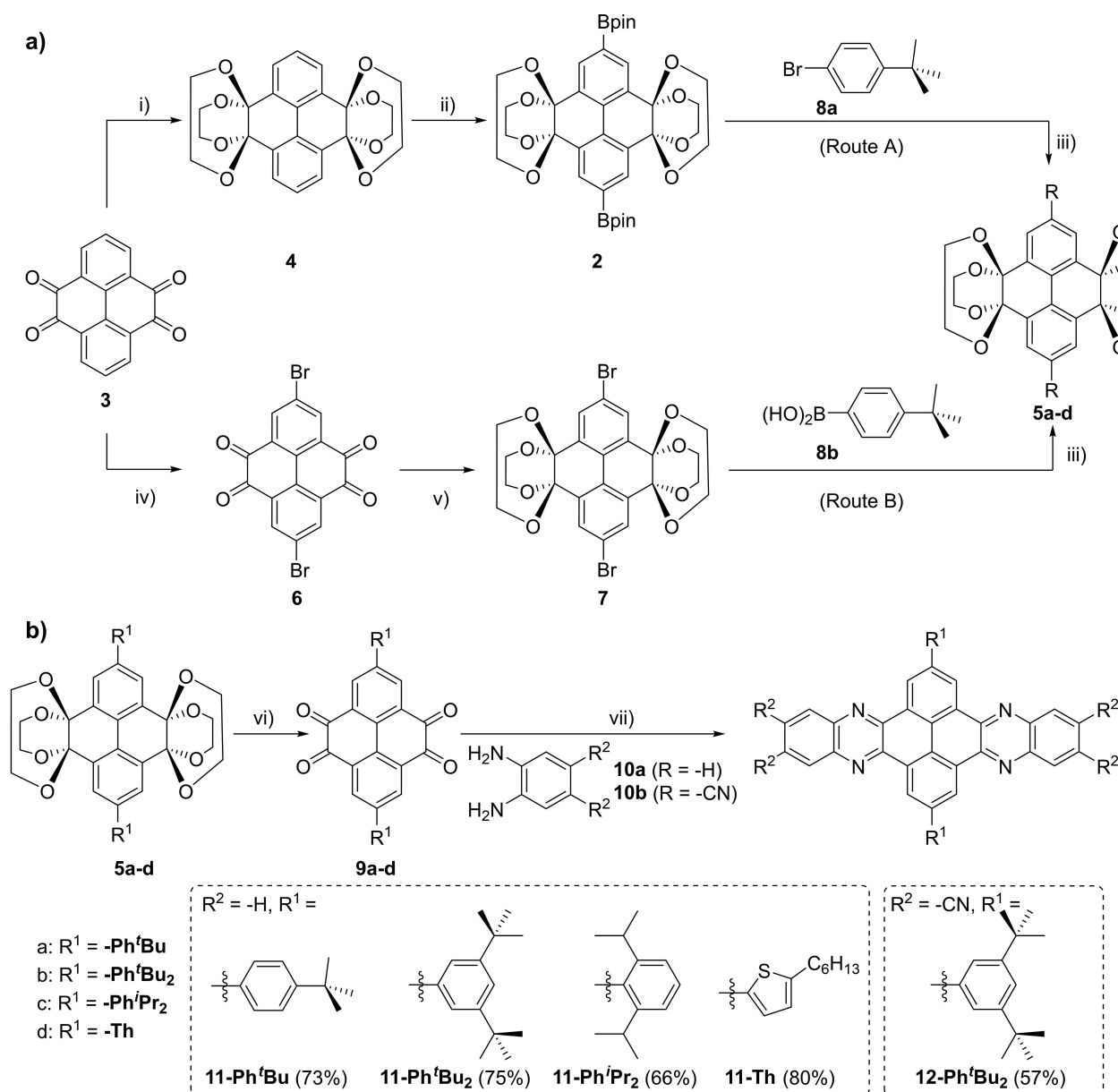
donating amino groups in shorter pyrazine derivatives were introduced by the group of Marder.^[55]

Here we report on QPP-based cruciforms based on diborylated tetraketal **2**^[55] as a versatile building block for Suzuki-Miyaura cross-coupling reactions to synthesize QPPs with aromatic substituents. Very recently, tetraketal **2** was used by the group of Dumele to synthesize Cyclo-2,7-pyrenylenes with confined space.^[56]

Results and Discussion

Synthesis and Characterization

Starting from pyrene tetraone **3** diborylated tetraketal **2** and dibrominated tetraketal **7** were synthesized according to literature known procedures.^{[55][7]} Subsequently, both compounds were tested for their suitability in Suzuki-Miyaura cross coupling reactions (Scheme 2a) by reacting either **2** with 4-*tert*-butylphenyl bromide (Route A) or **7** with the corresponding boronic acid **8** (Route B) under Fu conditions.^[57] While we found only poor conversion and a yield of about 10% of tetraketal **5a**



Scheme 2. a) Synthesis of pyrene tetraketal **5a** via two different routes A and B. Conditions: i) ethylene glycol, *p*-toluenesulfonic acid, toluene, 130 °C, 100 min. Dean-Stark trap, 82%. ii) B₂Pin₂, 5 mol-% [Ir(OMe)(COD)]₂, THF (abs.), Ar, 85 °C, 89%. iii) 5 mol-% Pd₂(dba)₃, 20 mol-% HP^tBu₃BF₄, THF, 1 M K₂CO₃ (aq.), 85 °C, 17 h, Ar (**5a** (82% via route A, 10% via route B), **b** (63%), **d** (45%)). For **5c**: 5 mol-% Pd(PPh)₄, 1,4-dioxane, 1 M K₂CO₃ (aq.), 85 °C, 17 h, Ar, 20%. iv) NBS, H₂SO₄ (conc.), 55 °C, 4.5 h, 56%. v) Ethylene glycol, *p*-toluenesulfonic acid, toluene, 135 °C, 3.5 h, molecular sieve, 83%. b) Synthesis of QPP derivatives. Conditions: vi) TFA/H₂O (9:1), 5–24 h, rt (100 °C for **9d**), 76–89%. vii) CHCl₃/AcOH, 70 °C, 17 h, Ar.

for Route B, under the same conditions much better yields (82%) could be isolated via Route A. The improved performance makes tetraketal **2** a versatile precursor for the synthesis of 2,7-diaryl-substituted pyrene tetraone derivatives via Suzuki-Miyaura cross-coupling.

Three other tetraketal derivatives with 3,5-di-*tert*-butylphenyl (**5b**), 2,6-di-*iso*-propylphenyl (**5c**) and 2-hexylthiophenyl (**5d**) substituents were synthesized as well via Route A. While **5b** and **5d** could be isolated in 63% and 45%, respectively, no reaction to **5c** was observed, probably due to steric hindrance of the *iso*-propyl substituents. After changing reaction conditions (Pd(PPh₃)₄, 1,4-dioxane) **5c** was obtained in 20% yield. The tetraketals were subsequently transformed under acidic conditions to tetraones **9a–d** in 76–89% yield (Scheme 2b). Thiophene-based tetraketal **9d** was more stable against acidic conditions compared to the other tetraketals, so that an increased reaction time and temperature (24 h, 100 °C) was required for complete conversion. Unlike the other products, **9d** was hardly soluble in common organic solvents (CHCl₃, CH₂Cl₂, TCE, THF, and DMSO) and could only be analyzed by NMR spectroscopy at elevated temperature (50 °C) in CDCl₃. In contrast to the other tetraones, **8d** did not show the typical orange-red color, but was deep blue instead. This suggests an intramolecular charge transfer between the electron-rich thiophenyl groups and the electron-withdrawing keto groups. All tetraketals and tetraones were characterized by ¹H and ¹³C NMR spectroscopy, mass spectrometry, FT-IR spectroscopy, and elemental analysis (see the Supporting Information).

Subsequently, a series of five QPP derivatives with aromatic substituents (4-*tert*-butylphenyl (–Ph^tBu), 3,5-di-*tert*-butylphenyl (–Ph^tBu₂), 2,6-di-*iso*-propylphenyl (–PhⁱPr₂), and 2-hexylthiophenyl (–Th)) at the pyrene moiety, were synthesized by acid-catalyzed condensation of tetraones **9a–d** with phenylenediamines **10a** and **10b** (Scheme 2b). In addition, a QPP tetracarbonitrile derivative bearing four cyano substituents (**12-Ph^tBu₂**) was synthesized by condensation with **9b** as well. The QPPs were obtained as yellow solids after washing with methanol in yields between 57–80%. With the exception of **11-Ph^tBu₂**, which was sufficiently soluble in common organic solvents for NMR spectroscopic studies (see the Supporting Information), all QPPs were poorly soluble in CHCl₃, CH₂Cl₂, tetrachloroethane, toluene, *o*-DCB, mesitylene, THF, CS₂, and pyridine. Benzoinitrile turned out to be a comparatively good solvent for all QPPs and was thus used for crystallization experiments (see discussion below). Due to low solubility **11-Ph^tBu**, **11-PhⁱPr₂**, **11-Th** and **12-Ph^tBu₂** could only be characterized by mass spectrometry, IR spectroscopy and elemental analysis. **11-Ph^tBu** is the only derivative with a decent solubility and could therefore also be analyzed by ¹H and ¹³C NMR spectroscopy (see the Supporting Information).

Crystals suitable for X-ray structural analysis were obtained of three tetraketal derivatives (**2**, **5a** and **7**) and two tetraone derivatives (**9a** and **9b**). For tetraone **9a** two modifications were obtained. Two different modifications of tetraketal **2** have previously been reported by the groups of Marder and Dumele.^[55–56]

In the structures of tetraketals **2** and **7** (Figure S47a–d) adjacent molecules stack in an edge-to-face arrangement with van der Waals contacts between the CH₂-protons of the ketal units and the pyrene plane ($d_{\text{CH}\cdots\pi} = 2.66\text{--}2.96 \text{ \AA}$). In the case of **7**, additional interactions between the bromine atoms and the aromatic protons with $d_{\text{CH}\cdots\text{Br}} = 2.75 \text{ \AA}$ are found (Figure S47d). Noteworthy, no π contacts between adjacent pyrene units are found in all tetraketal structures, suggesting that the tetraketal units efficiently suppress π -stacking.

Crystals of tetraone **9a** were grown by slow evaporation of a CHCl₃ solution. Two modifications were obtained. In polymorph α , the compound crystallized in the monoclinic space group C2/c with four molecules in the unit cell and half a molecule in the asymmetric unit. Adjacent molecules are stacked crosswise ($d_{\pi} = 3.43 \text{ \AA}$) over the phenylene substituents and the pyrene unit at an angle of 60°, forming a two-dimensional zigzag brick wall stacking motif along the crystallographic *b*-axis (Figure S47e,f). The structure is stabilized by hydrogen bonding between the carbonyl oxygens and the aromatic protons of the phenylene units ($d_{\text{A}} = 2.60\text{--}2.72 \text{ \AA}$). Short contacts between adjacent oxygen atoms also exist ($d_{\text{B}} = 3.12 \text{ \AA}$). Adjacent layers interact via dispersion interactions.

Polymorph β crystallized in the triclinic space group P-1 with three molecules in the asymmetric unit and six molecules in the unit cell. The packing strongly resembles the α -modification and only a slightly different orientation of adjacent molecules are found. The two-dimensional π -stacking motif is potentially capable of efficient two-dimensional charge transport. A charge transfer integral for electron transport along the π -stacking direction of 43 meV was calculated via the DFTB method^[58–64] (see the Supporting Information for computational details) making tetraone **9a** a promising candidate for semi-conducting electron transport. Table 1 gives an overview of crystallographic parameters.

Optoelectronic Properties of the QPPs

The frontier molecular orbitals were quantum-chemically calculated by DFT methods (B3LYP/6-311++G**) and are depicted in Figure 1. For all QPPs the LUMO orbitals are delocalized over the entire QPP backbone and are not affected by the aromatic substituents ($E_{\text{LUMO}} = -2.7$ to -2.8 eV). As expected, the cyano groups in **11-Ph^tBu₂** stabilize the LUMO ($E_{\text{LUMO}} = -3.8 \text{ eV}$). The HOMO orbitals are delocalized crosswise to the LUMOs across the pyrene unit and the aromatic substituents for all QPPs except **11-PhⁱPr₂**, because due to the attached isopropyl groups, the π -plane of the benzene ring is found orthogonal to that of the pyrene unit and thus does not allow any orbital overlap. **11-Ph^tBu**, **11-Ph^tBu₂**, and **11-Th** have almost identical HOMO energies ranging from $E_{\text{HOMO}} = -5.9$ to -5.8 eV . In **11-PhⁱPr₂** and **12-Ph^tBu₂**, the HOMOs are stabilized to $E_{\text{HOMO}} = -6.3$ and -6.6 eV , respectively. The electronic band gaps range from $E_{\text{g}} = 2.8 \text{ eV}$ for **12-Ph^tBu₂**, $E_{\text{g}} = 3.0 \text{ eV}$ for **11-Th**, $E_{\text{g}} = 3.2 \text{ eV}$ for **11-Ph^tBu** and **11-PhⁱPr**, and $E_{\text{g}} = 3.6 \text{ eV}$ for **11-PhⁱPr**. The calculated frontier orbital energies are in the same range as the

#	Cmpd.	Method	Space group (crystal system)	N_{asym} ^[c]	Z ^[d]	solvent ^[e]
1	2	CHCl ₃ /EtOH ^[a]	<i>Pca</i> 2 ₁ (orthorhomb.)	1	4	2 × CHCl ₃
2	7	CHCl ₃ ^[b]	<i>C2/c</i> (monoclinic)	1	8	–
3	5a	CHCl ₃ ^[b]	<i>P1</i> (triclinic)	1	2	2 × CHCl ₃
4	9a	CHCl ₃ ^[b] (α)	<i>C2/c</i> (monoclinic)	0.5	4	–
5		CHCl ₃ ^[b] (β)	<i>P1</i> (triclinic)	2 + 2 × 0.5	6	–
6	9b	CHCl ₃ ^[b]	<i>P1</i> (triclinic)	0.5	1	1 × CHCl ₃

[a] Vapor diffusion of the antisolvent (EtOH). [b] Slow evaporation at rt. [c] Number of molecules in the asymmetric unit, solvent molecules not counted. [d] Total number of molecules in the unit cell including resolved solvent molecules. [e] Number of resolved solvent molecules in the asymmetric unit.

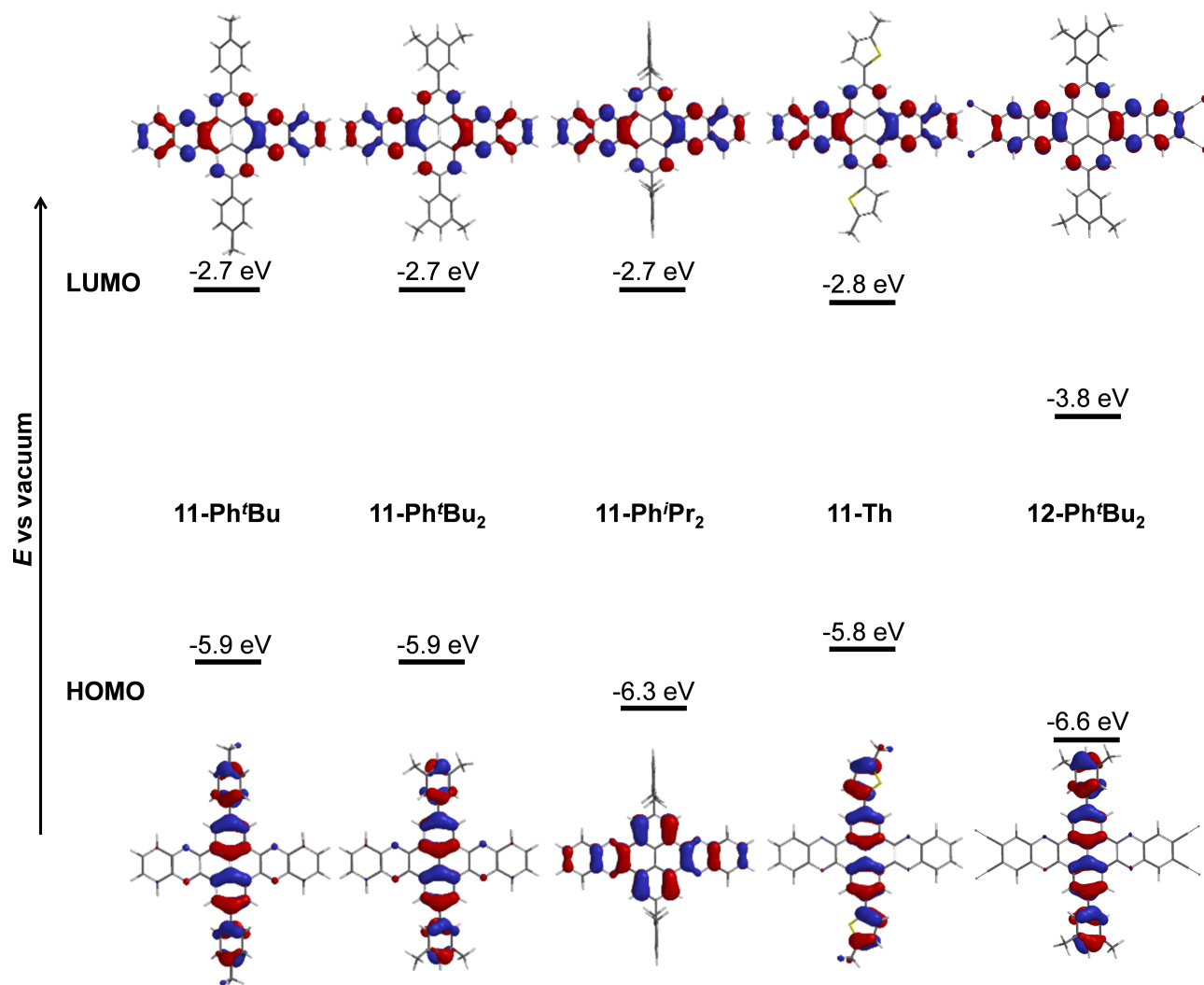


Figure 1. HOMO-LUMO diagram of pyrene-substituted QPPs calculated by DFT-B3LYP/ 6 311 + + G**. *tert*-butyl and hexyl groups were replaced by methyl groups to reduce the calculation time.

energies of *tert*-butyl substituted and unsubstituted derivatives.^[37,41–42]

The optical properties were investigated by absorption and emission spectroscopy in CHCl₃ (Figure 2). In the UV/Vis spectra, **11-Ph^tBu₂** and **11-PhⁱPr₂** show similar absorption maxima at $\lambda_{\text{abs}} = 417, 393, 373, 338, 315$ and 280 nm and at $\lambda_{\text{abs}} = 414, 390,$

$370, 328, 313,$ and 263 nm, respectively. In contrast, **12-Ph^tBu₂** shows significant red shifted *p*-bands at $\lambda_{\text{abs}} = 438$ and 414 nm and a β -band at $\lambda_{\text{abs}} = 393$ nm, respectively. The spectra of **11-Ph^tBu** and **11-Th** are less resolved. **11-Ph^tBu** shows only weak absorptions at $\lambda_{\text{abs}} = 417$ and 395 nm, and an elongated shoulder at ~ 575 nm. In the spectrum of **11-Th**, the bands at

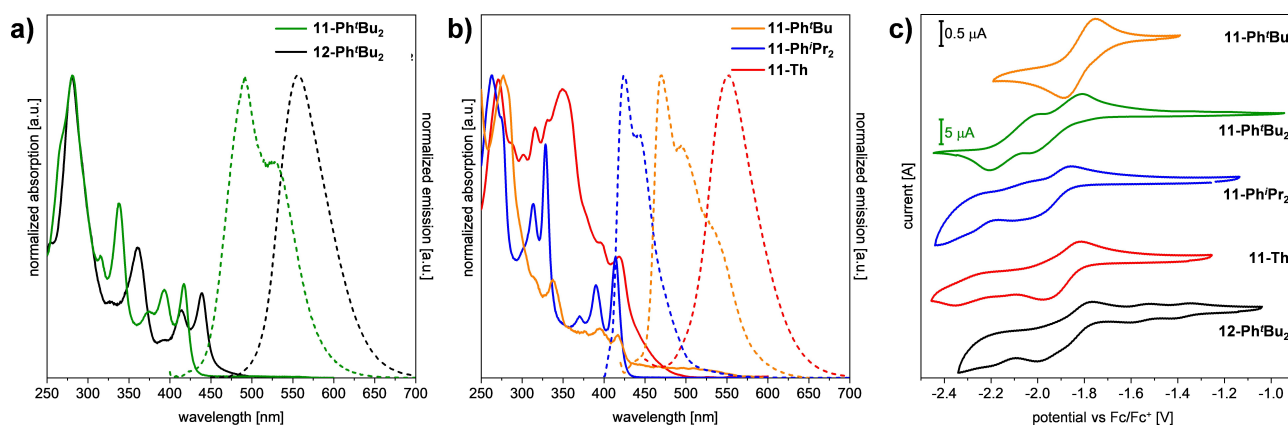


Figure 2. a,b) Absorption and emission spectra of pyrene-substituted QPPs measured in CH_2Cl_2 ($1 \mu\text{mol L}^{-1}$) at rt. c) Cyclic voltammograms (*o*-DCB, 0.1 mol L^{-1} $n\text{Bu}_4\text{NPF}_6$) of pyrene substituted QPPs measured at rt with a Pt working electrode, an Ag/Ag⁺ pseudo-reference electrode and Fc/Fc⁺ as internal reference (scan rate: 100 mV s^{-1}). The scale of the y-axis differs for **11-Ph'Bu**₂ due to the strongly increased signal intensity.

$\lambda_{\text{abs}}=418$ and 396 nm are partially overlapping with the strongly broadened β -band at $\lambda_{\text{abs}}=349 \text{ nm}$. The optical band gaps of the five QPP derivatives lie between $E_{\text{g,opt}}=2.7$ and 2.9 eV .

In the emission spectra, the fluorescence maxima shift bathochromically from **11-Ph'Pr**₂ ($\lambda_{\text{em}}=424 \text{ nm}$), over **11-Ph'Bu** ($\lambda_{\text{em}}=470 \text{ nm}$), **11-Ph'Bu**₂ ($\lambda_{\text{em}}=492 \text{ nm}$), **11-Th** ($\lambda_{\text{em}}=552 \text{ nm}$) towards **12-Ph'Bu**₂ ($\lambda_{\text{em}}=556 \text{ nm}$). Additional fine splitting of the emission is found in the spectra of **QPP-Ph'Bu** ($\lambda_{\text{em}}=494 \text{ nm}$), **11-Ph'Bu**₂ ($\lambda_{\text{em}}=524 \text{ nm}$) and **11-Ph'Pr**₂ ($\lambda_{\text{em}}=442 \text{ nm}$). The Stokes shifts increase from $E_{\text{Stokes}}=570 \text{ cm}^{-1}$ for **11-Ph'Pr**₂, 2704 cm^{-1} for **11-Ph'Bu**, 3656 cm^{-1} for **11-Ph'Bu**₂ and 4845 cm^{-1} for **12-Ph'Bu**₂ towards 5807 cm^{-1} for **11-Th**, indicating an increase in the reorganization energy from the transition from the first excited state to the ground state in that order.

The electrochemical properties were investigated by cyclic voltammetry in *o*-DCB (Figure 2c). **11-Ph'Bu** shows a single

reduction potential at $E_{\text{red}}=-1.8 \text{ V}$. For **11-Ph'Bu**₂ two potentials could be measured at $E_{\text{red}}=-1.9$ and -2.1 V . The voltammograms of the other three QPPs show weaker signals due to lower solubility and are less resolved. For **11-Ph'Pr**₂ and **11-Th** a reduction potential at $E_{\text{red}}=-2.0$ and -1.9 V , respectively, could be observed. **12-Ph'Bu**₂ shows very weak signals at $E_{\text{red}}=-1.4$ and -1.6 V and another potential at $E_{\text{red}}=-1.9 \text{ V}$. From the first reduction potentials, the electron affinities were estimated via the commonly used expression $EA=(E_{\text{red},1}+4.8) \text{ eV}$ and all lie in a similar range of $EA=-2.8 \text{ eV}$ for **11-Ph'Pr**₂, 2.9 eV for **11-Ph'Bu**₂ and **11-Th** and -3.0 eV for **11-Ph'Bu** and are in good correlation to the DFT-calculated LUMO levels. For **12-Ph'Bu**₂, a lower affinity of $EA=-3.4 \text{ eV}$ was determined as expected due to the cyano groups. Table 2 gives an overview of the optoelectronic properties of the pyrene-substituted QPPs.

Table 2. Optoelectronic properties of pyrene-substituted QPPs.

Cmpd.	$E_{\text{HOMO}}^{\text{[a]}}$ [eV]	$E_{\text{LUMO}}^{\text{[a]}}$ [eV]	$E_{\text{g}}^{\text{[a]}}$ [eV]	$\lambda_{\text{abs}}^{\text{[b,c]}}$ [nm]	$\lambda_{\text{onset}}^{\text{[c]}}$ [nm]	$E_{\text{g,opt}}^{\text{[d]}}$ [eV]	$\lambda_{\text{em}}^{\text{[c]}}$ (λ_{ex}) [nm]	$E_{\text{Stokes}}^{\text{[e]}}$ [cm^{-1}]	$E_{\text{red}}^{\text{[e]}}$ [V]	$EA^{\text{[f]}}$ [eV]
11-Ph'Bu	-5.9	-2.7	3.2	417	430	2.9	470 494 528 ^{sh} (400)	2704	-1.8	-3.0
11-Ph'Bu ₂	-5.9	-2.7	3.2	417	429	2.9	492 524 (397)	3656	-1.9 -2.1	-2.9
11-Ph'Pr ₂	-6.3	-2.7	3.6	414	425	2.9	424 442 (407)	570	-2.0	-2.8
11-Th	-5.8	-2.8	3.0	418	451	2.7	552 (397)	5807	-1.9	-2.9
12-Ph'Bu ₂	-6.6	-3.8	2.8	438	452	2.7	556 (400)	4845	-1.4 -1.6 -1.9	-3.4

[a] Determined by quantum-chemical calculations (DFT-B3LYP/6-311++G**). [b] Red-shifted absorption maximum. [c] Measured in CHCl_3 at rt. [d] Optical bandgap determined by the absorption onset, $E_{\text{g,opt}}=1242/\lambda_{\text{onset}}^{\text{e}}$. [e] CV measured in *o*-DCB with a Pt working electrode, Ag/Ag⁺ as pseudoreference electrode, and $n\text{Bu}_4\text{NPF}_6$ as electrolyte. Scanning speed: 100 mV s^{-1} , Fc/Fc⁺ was used as internal reference. [f] Electron affinity determined via $EA=(E_{\text{red},1}+4.8) \text{ eV}$. sh: shoulder.

Crystallization Experiments and Calculated Charge Transfer Integrals

The low solubility (with the exception of **11-Ph'Bu₂**) limited the crystallization possibilities. Benzonitrile proved to be a relatively good solvent for all compounds, and needle-shaped crystals of **11-Ph'Bu₂**, **11-Ph'Pr₂**, and **12-Ph'Bu₂** were obtained by thermal crystallization. However, they were also too small to be measured directly. Instead, they were added as seed crystals to saturated solutions of the respective compound in benzonitrile to grow larger crystals. By vapor diffusion of EtOH sufficiently large crystals for X-ray diffraction were obtained in the case of **11-Ph'Bu₂** (modification α). Another modification could be

obtained by evaporation of solvent from a CHCl₃ solution (solvate β).

From benzonitrile, **11-Ph'Bu₂** crystallized in the monoclinic space group *C2/c* with half a molecule in the asymmetric unit and four molecules in the unit cell (Figure 3a-c and Table 3). Solvent molecules are not included in the crystal lattice. From CHCl₃, the monoclinic space group *P2/c* was obtained with half a molecule in the asymmetric unit and two molecules in the unit cell (Figure 3d-f). In both structures, **11-Ph'Bu₂** forms one-dimensional π -stacks along the crystallographic *b* axis with $d_{\pi} = 3.34$ Å (α) and $d_{\pi} = 3.31$ Å (β), respectively, with similar arrangement of π -stacked dimers. The two structures differ in the relative arrangement of the π -stacked columns to each other. In the α -modification, QPP planes of adjacent stacks interact with

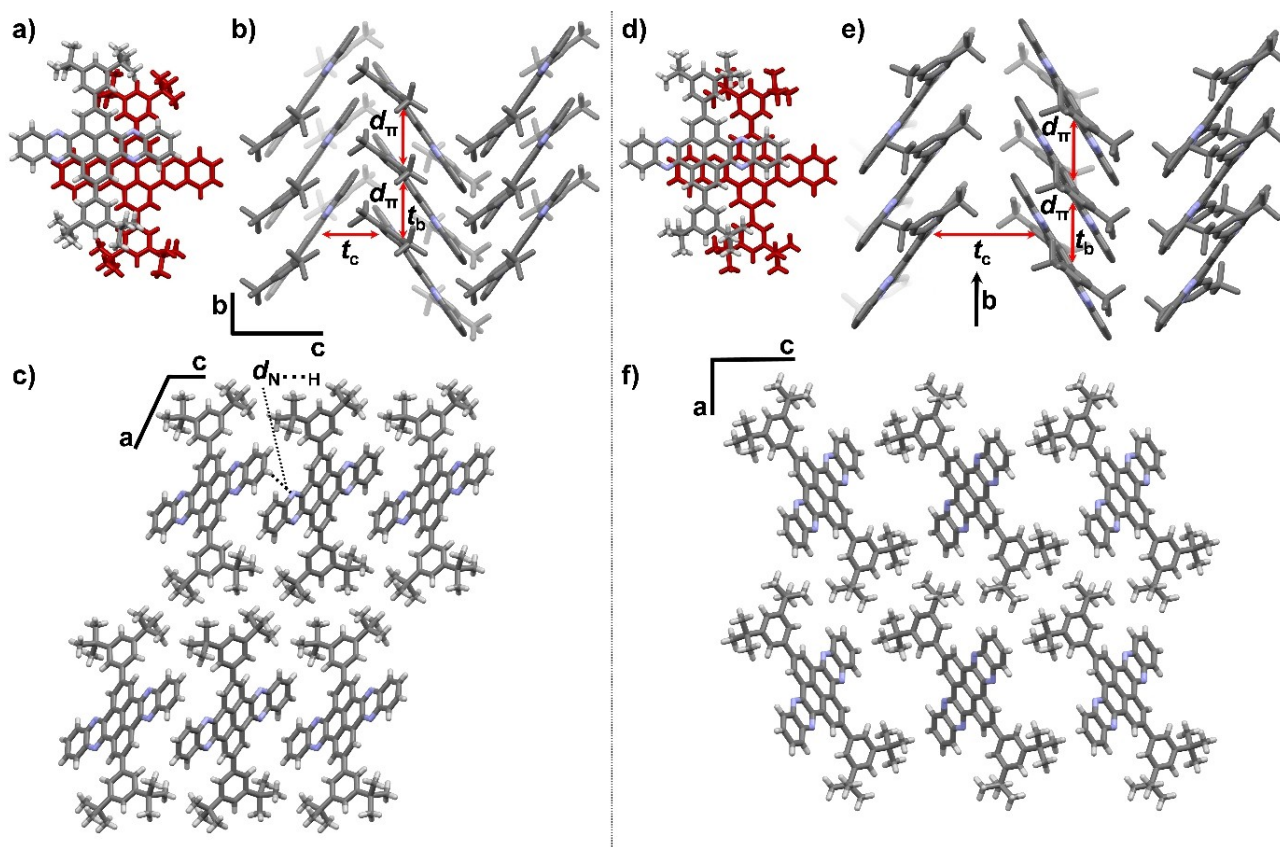


Figure 3. Single crystal X-ray structures of **11-Ph'Bu₂**. a-c) Polymorph α , crystallized by vapor diffusion of EtOH into a saturated benzonitrile solution with seed crystals ($d_{\pi} = 3.34$ Å, $d_{N \cdots H} = 2.72$ Å). d-f) Solvate β , crystallized by evaporation of a CHCl₃ solution ($d_{\pi} = 3.31$ Å). Solvent molecules and protons in (b) and (e) are omitted for clarity.

Table 3. Crystallographic parameters and calculated charge transfer integrals of **11-Ph'Bu₂** for hole (h) and electron (e) transport along the crystallographic *b* and *c* directions, respectively (see Figure 3).

Modification	Solvent	Space group (crystal system)	N_{asym} ^[a]	Z ^[b]	Transfer integral	<i>b</i> -axis (π stacking direction)	<i>c</i> -axis
α	Benzonitrile	<i>C2/c</i> (monoclinic)	0.5	4	t_h	15	7
					t_e	136	8
β	CHCl ₃	<i>P2/c</i> (monoclinic)	0.5	2	t_h	27	0
					t_e	73	0

[a] Number of molecules in the asymmetric unit, solvent molecules not counted. [b] Total number of molecules in the unit cell including resolved solvent molecules.

each other via contacts between the phenazine nitrogen atom and the peripheral phenylene proton with $d_{N\cdots H}=2.72 \text{ \AA}$, forming a layered structure within the crystallographic ac plane (Figure 3c). In contrast, adjacent stacks in the β modification interact via dispersion forces between the *tert*-butyl groups and the QPP unit (Figure 3f). The resulting cavities are filled with disordered solvent molecules.

The direct contact of the QPP planes in the α -modification is potentially advantageous, as it provides the possibility of two-dimensional charge transport. Transfer integrals for hole and electron transport have been calculated using the fragment orbital approach,^[58] which has been implemented for the semi-empirical density functional tight-binding method (DFTB).^[58–62] This method (for more details, see Supporting Information) has been benchmarked in detail in comparison to high-level ab-initio methods. Along the π stacking axis (*b*-axis), moderate hole transfer integrals of $t_h=15 \text{ meV}$ (α) and $t_h=27 \text{ meV}$ (β) were obtained for both crystal structures, respectively. In contrast, high couplings of $t_e=136 \text{ meV}$ (α) and $t_e=73 \text{ meV}$ (β) were calculated for electron transport. These values are in the same range as prominent benchmark organic semiconductors, such as rubrene (83 meV)^[63] or pentacene (75 meV).^[64] **11-Ph'Bu₂** thus represents a potential n-type semiconductor for OFETs. Along the *c*-axis, i.e. between molecules of neighboring π -stacks (Figure 3c,f), the transfer integrals for hole and electron transport are negligible in the β -modification, which is to be expected due to the lack of contact of the QPP planes. For the α -polymorph, the values along the *c*-axis are only slightly higher (7–8 meV). Accordingly, the charge transport should be strongly anisotropic in both modifications.

Conclusion

In summary, we have prepared a series of four aryl substituted pyrene substituted tetraones of a 2,7-diborylated pyrene tetraketal **2**, showing that **2** is a versatile building block for Suzuki-Miyaura cross-coupling reactions. X-ray crystallographic analysis of three tetraketal derivatives indicated that the tetraketal units efficiently prevent π stacking by sterically blocking the pyrene unit. Subsequently, five aryl substituted cruciform QPP derivatives were prepared by condensation of the tetraones with phenylene diamine or 4,5-diaminophthalonitrile. Except of di-*tert*-butylphenyl substituted QPP (**11-Ph'Bu₂**), which showed good solubility in common organic solvents, the other derivatives were only poorly soluble. The optoelectronic properties were investigated by absorption and emission spectroscopy, cyclic voltammetry and quantum-chemical calculations, showing that the LUMO energy levels are almost unaffected by the aryl substituents, but the HOMO level energy levels can be fine-tuned by the cruciform arrangements of these two FMOs. This enables the possibility to further fine tune optoelectronic properties more precisely for this interesting class of fused polycyclic aromatic compounds.

Two different crystal structures of **11-Ph'Bu₂** were obtained with similar, one-dimensional π stacked columns were obtained. Calculated charge transfer integrals (73–136 meV)

indicated that **11-Ph'Bu₂** is a promising material for n-type semiconducting charge transport. The presented synthetic route represents a versatile method towards aryl substituted QPPs and thus broadens the scope of easily accessible organic semiconductors. We are currently further investigating the scope of this method to synthesize new materials with efficient charge transport properties for OFET devices.

Experimental Section

For experimental details see the Supporting Information.

Deposition Numbers 2089480 (**2**), 2089481 (**7**), 2089482 (**5a**), 2089483 (**9a- α**), 2089484 (**9a- β**), 2089485 (**9b**), 2089486 (**QPP-Ph'Bu₂- α**), and 2089487 (**11-Ph'Bu₂- β**) contain the supplementary crystallographic data for this paper. These data are provided free of charge by the joint Cambridge Crystallographic Data Centre and Fachinformationszentrum Karlsruhe Access Structures service www.ccdc.cam.ac.uk/structures.

Acknowledgements

The authors are grateful to "Deutsche Forschungsgemeinschaft" supporting this project (within the collaborative research center SFB1249 "N-heteropolycyclic compounds as functional materials" (TP-A04, and TP-B02). Open Access funding enabled and organized by Projekt DEAL.

Conflict of Interest

The authors declare no conflict of interest.

Keywords: Charge transport · Cross-coupling · Nitrogen heterocycles · π Stacking · Quinoxalinophenanthrophenazines (QPPs)

- [1] C. R. Newman, C. D. Frisbie, D. A. da Silva Filho, J.-L. Brédas, P. C. Ewbank, K. R. Mann, *Chem. Mater.* **2004**, *16*, 4436–4451.
- [2] J. Zaumseil, H. Sirringhaus, *Chem. Rev.* **2007**, *107*, 1296–1323.
- [3] C. Wang, H. Dong, W. Hu, Y. Liu, D. Zhu, *Chem. Rev.* **2012**, *112*, 2208–2267.
- [4] Y. Wen, Y. Liu, *Adv. Mater.* **2010**, *22*, 1331–1345.
- [5] R.-P. Xu, Y.-Q. Li, J.-X. Tang, *J. Mater. Chem. C* **2016**, *4*, 9116–9142.
- [6] A. Salehi, X. Fu, D.-H. Shin, F. So, *Adv. Funct. Mater.* **2019**, *29*, 1808803.
- [7] M. Luo, H. Shadnia, G. Qian, X. Du, D. Yu, D. Ma, J. S. Wright, Z. Y. Wang, *Chem. Eur. J.* **2009**, *15*, 8902–8908.
- [8] M. Wang, H. Tong, Y. Cheng, Z. Xie, L. Wang, X. Jing, F. Wang, *J. Polym. Sci. Part A* **2010**, *48*, 1990–1999.
- [9] M. Wang, Y. Li, Z. Xie, L. Wang, *Sci. China Chem.* **2011**, *54*, 656–665.
- [10] Q. Li, J. Li, H. Ren, Z. Gao, D. Liu, *Synth. Commun.* **2011**, *41*, 3325–3333.
- [11] J. Wu, W. Pisula, K. Müllen, *Chem. Rev.* **2007**, *107*, 718–747.
- [12] W. Cao, J. Xue, *Energy Environ. Sci.* **2014**, *7*, 2123–2144.
- [13] E. Clar, R. Schoental, *Polycyclic hydrocarbons*, Springer, London, **1964**, p.
- [14] E. Clar, *Aromatic sextet*, Wiley, New York, **1972**, p.
- [15] A. Mateo-Alonso, N. Kulisic, G. Valenti, M. Marcaccio, F. Paolucci, M. Prato, *Chem. Asian J.* **2010**, *5*, 482–485.
- [16] N. Kulisic, S. More, A. Mateo-Alonso, *Chem. Commun.* **2011**, *47*, 514–516.
- [17] S. More, R. Bhosale, S. Choudhary, A. Mateo-Alonso, *Org. Lett.* **2012**, *14*, 4170–4173.
- [18] A. Mateo-Alonso, *Chem. Soc. Rev.* **2014**, *43*, 6311–6324.

- [19] S. More, R. Bhosale, A. Mateo-Alonso, *Chem. Eur. J.* **2014**, *20*, 10626–10631.
- [20] R. García, M. Melle-Franco, A. Mateo-Alonso, *Chem. Commun.* **2015**, *51*, 8037–8040.
- [21] A. B. Marco, D. Cortizo-Lacalle, C. Gozalvez, M. Olano, A. Atxabal, X. Sun, M. Melle-Franco, L. E. Hueso, A. Mateo-Alonso, *Chem. Commun.* **2015**, *51*, 10754–10757.
- [22] D. Cortizo-Lacalle, A. Pertegás, M. Melle-Franco, H. J. Bolink, A. Mateo-Alonso, *Org. Chem. Front.* **2017**, *4*, 876–881.
- [23] A. Mateo-Alonso, *Eur. J. Org. Chem.* **2017**, *2017*, 7006–7011.
- [24] J. Hu, D. Zhang, S. Jin, S. Z. D. Cheng, F. W. Harris, *Chem. Mater.* **2004**, *16*, 4912–4915.
- [25] X. Feng, F. Iwanaga, J.-Y. Hu, H. Tomiyasu, M. Nakano, C. Redshaw, M. R. J. Elsegood, T. Yamato, *Org. Lett.* **2013**, *15*, 3594–3597.
- [26] J. Guo, Y. Xu, S. Jin, L. Chen, T. Kaji, Y. Honsho, M. A. Addicoat, J. Kim, A. Saeki, H. Ihee, S. Seki, S. Irle, M. Hiramoto, J. Gao, D. Jiang, *Nat. Commun.* **2013**, *4*, 2736.
- [27] P. K. Sahoo, C. Giri, T. S. Haldar, R. Puttreddy, K. Rissanen, P. Mal, *Eur. J. Org. Chem.* **2016**, *2016*, 1283–1291.
- [28] B. R. Kaafarani, L. A. Lucas, B. Wex, G. E. Jabbour, *Tetrahedron Lett.* **2007**, *48*, 5995–5998.
- [29] B. Wex, A. a O. El-Ballouli, A. Vanvooren, U. Zschieschang, H. Klauk, J. A. Krause, J. Cornil, B. R. Kaafarani, *J. Mol. Struct.* **2015**, *1093*, 144–149.
- [30] J. Li, S. Chen, Z. Wang, Q. Zhang, *Chem. Rec.* **2016**, *16*, 1518–1530.
- [31] B.-L. Hu, K. Zhang, C. An, D. Schollmeyer, W. Pisula, M. Baumgarten, *Angew. Chem. Int. Ed.* **2018**, *57*, 12375–12379; *Angew. Chem.* **2018**, *130*, 12555–12559.
- [32] Y. Min, C. Dou, D. Liu, H. Dong, J. Liu, *J. Am. Chem. Soc.* **2019**, *141*, 17015–17021.
- [33] Y. Min, X. Cao, H. Tian, J. Liu, L. Wang, *Chem. Eur. J.* **2021**, *27*, 2065–2071.
- [34] Y. Min, C. Dou, H. Tian, J. Liu, L. Wang, *Chem. Eur. J.* **2021**, *27*, 4364–4372.
- [35] B. Kohl, F. Rominger, M. Mastalerz, *Org. Lett.* **2014**, *16*, 704–707.
- [36] B. Kohl, F. Rominger, M. Mastalerz, *Chem. Eur. J.* **2015**, *21*, 17308–17313.
- [37] F. Maass, A. Stein, B. Kohl, L. Hahn, L. H. Gade, M. Mastalerz, P. Tegeder, *J. Phys. Chem. C* **2016**, *120*, 2866–2873.
- [38] B. Kohl, M. V. Bohnwagner, F. Rominger, H. Wadepohl, A. Dreuw, M. Mastalerz, *Chem. Eur. J.* **2016**, *22*, 646–655.
- [39] E. Prantl, B. Kohl, D. Ryvlin, P. Biegger, H. Wadepohl, F. Rominger, U. H. F. Bunz, M. Mastalerz, S. R. Waldvogel, *ChemPlusChem* **2019**, *84*, 1239–1244.
- [40] B. Kohl, K. Baumgärtner, F. Rominger, M. Mastalerz, *Eur. J. Org. Chem.* **2019**, *2019*, 4891–4896.
- [41] L. Ueberricke, D. Holub, J. Kranz, F. Rominger, M. Elstner, M. Mastalerz, *Chem. Eur. J.* **2019**, *25*, 11121–11134.
- [42] L. Ueberricke, S. Wieland, F. Rominger, M. Mastalerz, *Organic Materials* **2019**, *01*, 050–062.
- [43] L. Ueberricke, I. Ciubotaru, F. Ghalami, F. Mildner, F. Rominger, M. Elstner, M. Mastalerz, *Chem. Eur. J.* **2020**, *26*, 11634–11642.
- [44] L. Ueberricke, F. Ghalami, W.-S. Zhang, V. Rao, F. Rominger, R. R. Schröder, M. Elstner, M. Mastalerz, *Cryst. Growth Des.* **2021**, *21*, 1329–1341.
- [45] L. Ueberricke, B. P. Benke, T. Kirschbaum, S. Hahn, F. Rominger, U. H. F. Bunz, M. Mastalerz, *Chem. Eur. J.* **2021**, *27*, 2043–2049.
- [46] L. Ueberricke, M. Mastalerz, *Chem. Rec.* **2021**, *21*, 558–573.
- [47] B. Gao, M. Wang, Y. Cheng, L. Wang, X. Jing, F. Wang, *J. Am. Chem. Soc.* **2008**, *130*, 8297–8306.
- [48] K. K. McGrath, K. Jang, K. A. Robins, D.-C. Lee, *Chem. Eur. J.* **2009**, *15*, 4070–4077.
- [49] L. V. Brownell, K. Jang, K. A. Robins, I. C. Tran, C. Heske, D.-C. Lee, *Phys. Chem. Chem. Phys.* **2013**, *15*, 5967–5974.
- [50] J. N. Wilson, M. Josowicz, Y. Wang, U. H. F. Bunz, *Chem. Commun.* **2003**, 2962–2963.
- [51] A. J. Zuccherro, J. N. Wilson, U. H. F. Bunz, *J. Am. Chem. Soc.* **2006**, *128*, 11872–11881.
- [52] A. J. Zuccherro, P. L. McGrier, U. H. F. Bunz, *Acc. Chem. Res.* **2010**, *43*, 397–408.
- [53] V. Martínez-Martínez, J. Lim, J. Bañuelos, I. López-Arbeloa, O. Š. Miljanić, *Phys. Chem. Chem. Phys.* **2013**, *15*, 18023–18029.
- [54] M. A. Saeed, H. T. M. Le, O. Š. Miljanić, *Acc. Chem. Res.* **2014**, *47*, 2074–2083.
- [55] J. Merz, M. Dietz, Y. Vonhausen, F. Wöber, A. Friedrich, D. Sieh, I. Krummenacher, H. Braunschweig, M. Moos, M. Holzapfel, C. Lambert, T. B. Marder, *Chem. Eur. J.* **2020**, *26*, 438–453.
- [56] N. Grabicki, K. T. D. Nguyen, S. Weidner, O. Dumele, *Angew. Chem. Int. Ed.* **2021**, *60*, 14909–14914.
- [57] A. F. Littke, C. Dai, G. C. Fu, *J. Am. Chem. Soc.* **2000**, *122*, 4020–4028.
- [58] A. Troisi, G. Orlandi, *J. Phys. Chem. A* **2006**, *110*, 4065.
- [59] A. Kubas, F. Hoffmann, A. Heck, H. Oberhofer, M. Elstner, J. Blumberger, *J. Chem. Phys.* **2014**, *140*, 104105.
- [60] A. Kubas, F. Gajdos, A. Heck, H. Oberhofer, M. Elstner, J. Blumberger, *Phys. Chem. Chem. Phys.* **2015**, *17*, 14342–14354.
- [61] B. Aradi, B. Hourahine, T. Frauenheim, *J. Phys. Chem. A* **2007**, *111*, 5678–5684.
- [62] M. Halder, S. Datta, P. Bolel, N. Mahapatra, S. Panja, H. Vardhan, S. Kayal, D. K. Khatua, I. Das, *Anal. Methods* **2016**, *8*, 2805–2811.
- [63] V. Coropceanu, J. Cornil, D. A. da Silva Filho, Y. Olivier, R. Silbey, J.-L. Brédas, *Chem. Rev.* **2007**, *107*, 926–952.
- [64] F. Valiyev, W.-S. Hu, H.-Y. Chen, M.-Y. Kuo, I. Chao, Y.-T. Tao, *Chem. Mater.* **2007**, *19*, 3018–3026.

Manuscript received: June 14, 2021
Revised manuscript received: July 21, 2021
Accepted manuscript online: July 27, 2021